Journal of Ovarian Research

RESEARCH

Open Access

# Near-infrared fluorescent molecular probes with cetuximab in the in vivo fluorescence imaging for epithelial ovarian cancer

Chen Zhang[1], Hongyan Cheng[1], Sha Dou[1], Yuanfen Wang[1], Xue Ye[1], Heng Cui[1*†], Xiaohong Chang[1*†] and Yi Li[1*†]

## Abstract

**Background** Near-infrared fluorescence (NIRF) imaging is an excellent choice for image-guided surgery due to its simple operation and non-invasiveness. Developing tumor-specific fluorescent molecular probes is key to fluorescence imaging-guided surgery. EGFR (epidermal growth factor receptor) is closely related to the proliferation and growth of tumor cells and is highly expressed in epithelial ovarian cancer (EOC). The study aims to construct a NIR fluorescent molecular probe using cetuximab (an EGFR monoclonal antibody) and investigate its feasibility for targeting EOC in vivo through fluorescence imaging.

**Methods** We determined the expression of EGFR in EOC. NIR fluorescent molecular probe with cetuximab (cetuximab-Cy7) was chemically engineered and identified. The subcutaneous xenografted tumor model of EOC was induced using SKOV3-Luc cell line with positive expression of EGFR. Cetuximab-Cy7 was used for in vivo fluorescence imaging, and phosphate-buffered saline, free Cy7 dye and mouse isotype immunoglobulin G-Cy7 were used as controls. NIRF imaging system was performed to study the distribution and targeting of the probes. Tumors were imaged in situ and ex vivo, and fluorescent intensity was quantified. Resected specimens were analyzed to confirm diagnosis, and immunohistochemical (IHC) staining was used to identify EGFR expression.

**Results** EGFR expression was increased in EOC tissues than fallopian tube tissues. The high expression of EGFR was significantly correlated with well-differentiation, residual lesions ≤ 1 cm, no recurrence and increased survival. NIRF imaging showed that the cetuximab-Cy7 enabled detection of tumor lesions in EOC-bearing mice with the optimal dose of 30 μg. The suitable imaging time window may be 24–96 h post-injection. Ex vivo fluorescence imaging indicated that fluorescent signal was mainly detected in the tumor and the lung. IHC results confirmed that xenografts were EGFR positive.

†Yi Li, Xiaohong Chang and Heng Cui jointly directed this work and should be considered as co-corresponding authors.

*Correspondence:
Heng Cui
cuiheng20@163.com
Xiaohong Chang
changxiaohong@pkuph.edu.cn
Yi Li
liyi@pkuph.edu.cn

Full list of author information is available at the end of the article

**Conclusion** Cetuximab-Cy7 can specifically target the tumors of EOC xenografted nude mice. This research lays the foundation for future studies on EOC surgery navigation.

**Keywords** Epithelial ovarian cancer, Near-infrared fluorescence imaging, Cetuximab, Cy7, Animal model

## Introduction

With estimated 19,680 new cases and12,740 deaths in USA in 2024, ovarian cancer (OC) remains one of the deadliest cancers in women [1]. OC is a heterogeneous group of malignant tumors with distinct differences in etiology, morphology, biological behavior, and molecular characteristics among different histopathological types, with approximately 90% being epithelial ovarian cancers (EOC). Surgery is the cornerstone of treatment of OC. The completeness of surgery is an independent prognostic factor impacting survival [2, 3]. Therefore, it is crucial to reduce the tumor burden. Even if complete resection is impossible, every effort should be made to minimize the tumor burden. However, achieving satisfactory cytoreduction (no visible residual tumor or residual tumor diameter ≤ 1 cm) can be challenging due to the fact that surgeons mainly rely on imprecise visual inspection and empirical tactile feedback to determine tumor margins [2]. There is an urgent need to investigate highly accurate and real-time intraoperative methods for tumor delineation.

Fluorescence-guided surgery (FGS) has emerged as a promising imaging method that provides surgeons with real-time intraoperative guidance for tumor visualization and delineation in surgery for cancers including OC [4, 5]. Based on robust studies, fluorescence imaging agents including 5-aminolevulinic acid and indocyanine green has been already approved for clinical use by the US Food and Drug Administration [4]. However, conventional fluorescence imaging agents showed significant limitations with less molecular specificity and image contrast. In recent decades, increasing evidence indicated that the tumor-specific fluorescent agents conjugating the fluorophores and various targeted ligands, such as small molecules, peptides and antibodies, showed translational potential in surgical navigation for various cancer types. Near-infrared fluorescence (NIRF) emitters have been widely used for real-time intraoperative imaging owing to deeper tissue penetration and better tumor-to-background (T/B) ratio [5].

So far, the folate receptor α (FRα)-targeting strategy has been explored most for OC imaging. FRα is considered to be a great potential tumor-associated antigen with overexpression in 90-95% EOC [6, 7], and its expression is significantly correlated with histological grade and stage [8, 9]. Pafolacianine (OTL38) is a conjugate of a folic acid coupled to a NIR fluorescent dye. A series of clinical trials showed that pafolacianine could intraoperatively discriminate cancers from normal tissues [10, 11]. Especially in the latest phase III study, it detected additional cancer on tissue not suspected by visual assessment and palpation in 33% FR-positive OC patients [11]. However, a high false positive rate (fluorescence positive but not confirmed by pathology) was noted [11]. It proposed that the false positive fluorescence may be caused by pafolacianine binding to FRβ + macrophages in the lymph nodes. Thus, there is no completely satisfactory molecular imaging probe and still an unmet need to create more innovative molecular probes.

EGFR (epidermal growth factor receptor), a member of HER (human epidermal growth factor receptor) family, is a universal biomarker for tumors and involved in the proliferation and growth of tumor cells. Literature reports indicate varying expression rates of EGFR in OC, ranging from 4 to 100% [12] or 70-100% [13], with some suggesting an average expression rate around 48% [12]. A study showed that high expression of EGFR was associated with elder age, advanced disease stage, poor differentiation, metastasis, and residual disease after surgery in OC [14]. Forlani L et al. proposed that EGFR could be a prognostic biomarker in OC and contribute to stratify OC patients [15]. Moreover, EGFR may be important in driving chemoresistance in the EOC cells through MEKK signal pathways [16]. Increasing studies indicated that EGFR phosphorylation or hyperactive EGFR signaling contribute to cisplatin resistance in OC [17–21]. However, there is no consensus regarding the expression status of EGFR in relation to OC and its implications [12, 14].

This study aims to use tissue microarrays (TMAs) for immunohistochemical (IHC) detection of EGFR expression in EOC tissues, and apply immunofluorescence (IF) techniques to screen for EGFR-positive cell lines to construct xenograft tumor models. We developed a NIR fluorescent molecular probe conjugated with cetuximab (an EGFR monoclonal antibody) to investigate its feasibility in in vivo fluorescence imaging of OC xenograft tumor models (Fig. 1). The fluorescent molecular probes specifically targeting EGFR developed in this study will extend visualization time and enhance image specificity, thereby contributing to the establishment of novel methods for resection of lesions, and eventually transforming surgical approaches in the treatment of OC.

## Materials and methods

### Antibodies and reagents

Rabbit monoclonal antibody against the EGFR used in IHC staining (1:100), western blotting (WB) (1:4000) and IF staining (1:300) analyses was from Abcam (ab52894).

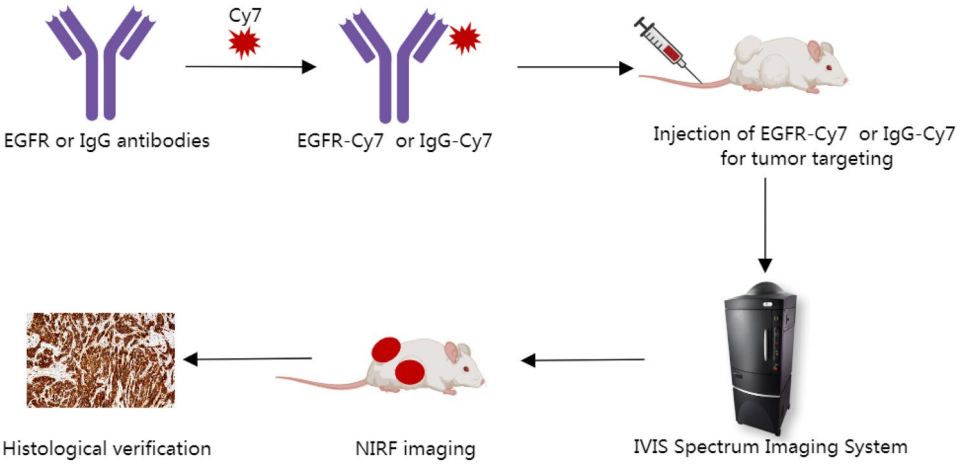


**Fig. 1** Scheme for using cetuximab-Cy7 probe in NIRF guided surgery in OC. EGFR-Cy7: epidermal growth factor receptor-cyanine7 (cetuximab-cyanine7); NIRF: near-infrared fluorescence; OC: ovarian cancer; IgG-Cy7: immunoglobulin G-cyanine7

Mouse monoclonal anti-β-tubulin antibody (1:1000) used as a loading control in WB analysis was from Cell Signaling Technology (#86298). Secondary antibody from Abcam (ab150079; 1:1000) for EGFR was used in IFstaining. A goat anti-rabbit secondary antibody (ab216773; 1:10000) for EGFR, and a goat anti-mouse secondary antibody (ab216776; 1:10000) for β-tubulin were used in WB analysis. Cy7 Nhydroxysuccinimide (NHS) ester (Lumiprobe, Hunt Valley, MD, USA) was employed to label commercially available EGFR monoclonal antibody cetuximab (Erbitux, Merck Lyon, Germany) and the mouse isotype immunoglobulin G (IgG) antibody (ZDR-5006, ZSGB-BIO, Beijing, China) which was used as control in NIRF imaging.

### Cells

The OC cell lines SKOV3·ip1, OVCAR3, A2780, 3AO, OV420, OV429 and ES2 preserved in Center of Gynecologic Oncology, Peking University People's Hospital were cultured in RPMI-1640 medium with 10–20% fetal bovine serum (FBS) and 1% penicillin/streptomycin (PS). HeLa cell line was cultured in DMEM medium with 10% FBS and 1% PS, and SKOV3 cell line in McCoy's 5 A medium with 10% FBS and 1% PS. The SKOV3-Luc cell line genetically labeled using a firefly luciferase reporter gene was provided by Professor Xipeng Wang from Shanghai Jiao Tong University and cultured in RPMI-1640 medium with 10% FBS and 1% PS. The cells were cultured in a 5% CO2 incubator at 37 °C.

### TMA and IHC staining with EGFR

A previously described TMA with duplicate cores from 420 OC and 112 fallopian tube (FT) tissues was obtained from Qilu Hospital of Shandong University [22]. IHC staining was conducted as previously described [22]. Evaluation of EGFR staining intensity was performed using H-score system [22]. The DensitoQuant module of Quant Center software (3DHISTECH Ltd., Budapest, Öv u. 3., Hungary) was used to automatically and quantitatively measure the H-score, which ranges from 0 to 300. The H-scores of duplicate cores were averaged. The receiver-operating characteristic (ROC) curve analysis [22, 23] provided the optimal cut-off value for H-score. The threshold for EGFR expression was set at 96.83. A score > 96.83 was classified as EGFR-high expression group, while ≤ 96.83 was EGFR-low expression group.

### Quantitative real-time PCR (qPCR) analysis of EGFR mRNA expression

Total RNA from cells was extracted by TRIzol reagent (Invitrogen). The cDNA was synthesized from 1 μg of total RNA in a 20 μl reaction volume using a FastQuant RT Kit (with gDNase) (Tiangen Biotech, Beijing, China). The qPCR reaction was performed in a Bio-Rad CFX real time PCR system in triplicate using the Power SYBR® Green PCR Master Mix Kit (Applied Biosystems, Austin, TX, USA). The gene-specific primers used for amplification were as follow: GAPDH, 5'-GCACCACCAACTG CTTAGC-3' (forward) and 5'-GGCATGGACTGTGG TCATGAG-3' (reverse); EGFR 5'- GTGTGCCACCTG TGCCATCC-3' (forward) and 5'- GCCACCACCAGC AGCAAGAG-3' (reverse). Relative expression of EGFR to GAPDH were measured by the $2^{-\Delta\Delta Ct}$ method. The experiment was repeated in triplicate.

### WB analysis of EGFR protein expression

Cells were lysed in radio immunoprecipitation assay lysis buffer (RIPA) buffer (Cell Signaling Technology, Danvers, MA, USA) supplemented with phenylmethanesulfonyl fluoride (PMSF; Cell Signaling Technology, Danvers, MA, USA) to extract total proteins. The lysate was centrifuged at 13,000 x g for 20 min at 4 °C and

protein concentrations were detected on the supernatant using Bradford assay (Bio-rad, Hercules, CA, USA). Equal amounts of protein obtained from different cell lysates were electrophoresed with 10% sodium dodecyl sulfate - polyacrylamide gel electrophoresis (SDS-PAGE) gels and then were transferred to polyvinylidene fluoride membranes (Millipore Corporation, Bedford, MA, USA). Membranes were incubated overnight at 4 °C with primary bodies in blocking buffer. The next day, membranes were washed and incubated with secondary antibody. Protein band intensities were scanned using a Licor Odyssey Imaging System (Lincoln, Nebraska, USA) and determined using Image-J software (NIH). The experiment was repeated three times.

#### IF staining with EGFR

Cells were cultured on 24-well plates until 50–70% confluence. After phosphate-buffered saline (PBS) washing, the cells were fixed in 4% paraformaldehyde (PFA) for 15 min, permeabilized with 0.2% TritonX-100 for 10 min, and incubated with blocking buffer of 1% bull serum albumin (BSA; Solarbio, Beijing, China) for 30–60 min. Then cells were incubated with primary antibodies overnight at 4 °C. The primary antibodies were removed the next day and the secondary antibodies were added to the cells at room temperature for 30–60 min. Cells were then stained with 4′,6-diamidino-2-phenylindole (DAPI; Solarbio, Beijing, China) to identify cell nuclei. Covered with 90% glycerolanalyzed to seal tablet, the cells were imaged with a fluorescence microscope (Carl Zeiss, Leica, DM IL LED, Germany). The images with different color channels were merged by Image-J software.

#### Synthesis and characterization of the cetuximab-Cy7 probe

The fluorescent dye Cy7 NHS ester (Lumiprobe, Hunt Valley, MD, USA) was employed to label cetuximab or control mouse isotype IgG antibody according to a previously reported protocol [22]. The Cy7 dye was added to the antibodies at a molar ratio of 20:1, and reacted in boric acid/NaOH (pH: 8.3−8.5) at 4 °C in the dark overnight. After the reaction, the mixture was purified using a Zeba Spin Desalting Column, 0.5 mL, 7 K MWCO (Thermo Fisher Scientific, Rockford, IL, USA). A UV-Vis system (Thermo Fisher Scientific) was used to measure the absorbance of the samples at 280 nm to detect protein concentrations and at 750 nm to determine the number of fluorophore molecules conjugated to each antibody. In parallel, the Cy7 labeling was evaluated by SDS-PAGE using a NIRF imaging system.

#### Animal models and treatment groups

To induce OC subcutaneous xenograft tumor models, 4- to 5- week-old BALB/c female nude mice were inoculated with $5\times10^6$ SKOV3-Luc cells suspended in 100 μL PBS into the right axilla. Tumor sizes were regularly and continuously measured with a caliper and calculated by using the following formula: length×width$^2\times0.5$ [24]. Tumors were allowed to grow to 100−500 mm$^3$ prior to NIRF imaging. The mice were randomly divided into 10 groups and intravenously injected with 100 μL of the following agents via the tail-vein: (1) PBS; (2) free Cy7; (3) 1.1 μg IgG-Cy7; (4) 3.3 μg of IgG-Cy7; (5) 10 μg IgG-Cy7; (6) 30 μg IgG-Cy7; (7) 1.1 μg cetuximab-Cy7; (8) 3.3 μg cetuximab-Cy7; (9) 10 μg cetuximab-Cy7; and (10) 30 μg cetuximab-Cy7 ($n=3$ per group). It should be noted that the control groups (1) −(6) were also used in our previous study [22] and we have got permission from the journal publisher (as shown in attached materials).

#### In vivo bioluminescence and NIRF imaging in EOC animals

Mice were kept anesthetized with 5% isoflurane. Bioluminescent imaging (BLI) was performed to assess tumor formation in mice of SKOV3-Luc cell xenografts 10 min after intraperitoneal injection of D-luciferin (150 mg/kg). BLI and NIRF imaging in xenograft models with lateral and ventral positions were conducted at 4, 24, 48, 96, 144, 192 and 264 h after injection with corresponding agents via the tail vein using IVIS Spectrum Imaging System (Xenogen, Alameda, CA, USA). The same fixed black board used when imaging was taken as the background to eliminate possible interference. The region of interest (ROI) on the tumors and background was analyzed and quantified with IVIS software. The T/B ratio was calculated using the formula $ROI_{tumor}/ROI_{background}$ ($n=3$ per group).

#### Ex vivo NIRF imaging of cetuximab-Cy7 and EGFR expression of tumor samples

Mice were sacrificed and dissected after imaging. The organs including heart, lung, liver, spleen, kidney, ovary, fallopian tube and uterus, and tumors were subjected to ex vivo NIRF imaging using IVIS Spectrum Imaging System. Surgical excised organs and tumors were fixed in 4% PFA and embedded in paraffin. The tumors were simultaneously stained with hematoxylin-eosin (H&E) and immunohistochemistry of EGFR to verify the presence of EOC and expression of EGFR in tumor implants.

#### Statistics

Quantitative data were presented as the means±standard deviation of three replicate experiments or three technical replicates from individual experiments. Kolmogorov-Smirnov test was used to test normality. EGFR expression in TMAs assay was assessed by Pearson's Chi-square test. Variations among multiple groups were evaluated using two-way analysis of variance (ANOVA) test. A value of $p<0.05$ indicates significant. IBM SPSS

Statistics (Version 20.0; IBM Corp., New York, USA) was applied for statistical analysis.

## Results

### Conjugation and characterization of cetuximab-Cy7 probe

The cetuximab, a commercially available EGFR antibody, and mouse isotype IgG antibody were fluorescently labeled by conjugation of lysine residues with the N-hydroxy succinimide of Cy7 and were identified by UV spectroscopy and SDS-PAGE. The IgG antibody was used as control to exclude nonspecific binding. UV-Vis system showed that the number of Cy7 fluorophores attached to each IgG or EGFR molecule was approximately 2–3. As shown in Fig. 2A, the Cy7-labeled EGFR antibody solution displayed fluorescent signals under NIRF imaging. After SDS-PAGE of Cy7-labeled antibodies, the gel was scanned using the IVIS Spectrum Imaging System. No bands were observed under bright-field condition (Fig. 2B), but fluorescent bands for IgG-Cy7 and cetuximab-Cy7 were detected under NIRF imaging (Fig. 2C). These results indicated successful conjugation of Cy7 dye to the antibodies.

### EGFR expression in EOC tissues and cells

First, the higher EGFR expression (H-score > 96.83) in tumor tissues compared to FT tissues was detected with IHC staining using TMAs [41.7% (175/420) vs. 17.0% (19/112); $p=0.000$] (Fig. 3A; Table 1). EGFR antibody staining was mainly located on the cytomembrane, followed by the cytoplasm (Fig. 3A). The clinical relevance of EGFR in EOC was determined. EGFR expression was higher in serous subtype (43.7%; 162/371) than in non-serous subtype (22.7%; 10/44) ($p=0.008$) (Table 2). Meanwhile, the high expression of EGFR was significantly associated with well-differentiation (grade 1) ($p=0.001$), residual lesions ≤ 1 cm ($p=0.000$), no recurrence ($p=0.000$), and prolonged survival ($p=0.002$). However, EGFR expression did not show significant correlation with age, menopausal status, FIGO staging, lymph node metastasis, ascites, preoperative CA-125 value, and platinum resistance status (all $p>0.05$).

As shown in the qPCR experiments, EGFR expression was increased in SKOV3, OVCA429 and SKOV3·ip1 cell lines, but reduced in OVCAR3 and A2780 cell lines (Fig. 3B). In consistent with qPCR results, representative images and quantification analysis of WB indicated that EGFR expression was highest in SKOV3, followed by OVCA429 and SKOV3·ip1 (Fig. 3C-D). To verify and explore the localization of EGFR, IF staining was performed in the SKOV3 cells with high EGFR expression and the A2780 cells with low expression. Similar to the above-mentioned results, EGFR staining was predominantly distributed in the membrane of SKOV3 cells, while the staining in A2780 cells was extremely weak (Fig. 3E). These results showed that EGFR may serve as an attractive target for imaging of EOC. Therefore, we selected the SKOV3 cells for subsequent in vivo imaging experiments.

### In vivo imaging of EOC xenografts with cetuximab-Cy7

Subcutaneous tumor formation and location in mice of SKOV3 cell xenografts was accurately detected by BLI on an IVIS Spectrum system (Fig. 4A). To exclude the influence of Cy7 dye on imaging, we set up a control group with free Cy7 dye. According to Fig. 4B-C, the fluorescent signals in free Cy7 group could be detected at 4 h post injection (hpi), but disappeared at 24 hpi. It indicates that the Cy7 dye can be cleared from the body within 24 h and does not undergo nonspecific adsorption at the tumor site. No significant Cy7 fluorescent signals were detected in the PBS group at the indicated time points. Importantly, the fluorescent signals in the IgG-Cy7 groups never accumulated at the tumor site. As can be seen from the ventral position imaging in Fig. 4C, IgG-Cy7 was primarily metabolized through abdominal metabolic organs such as liver, spleen, and kidneys.

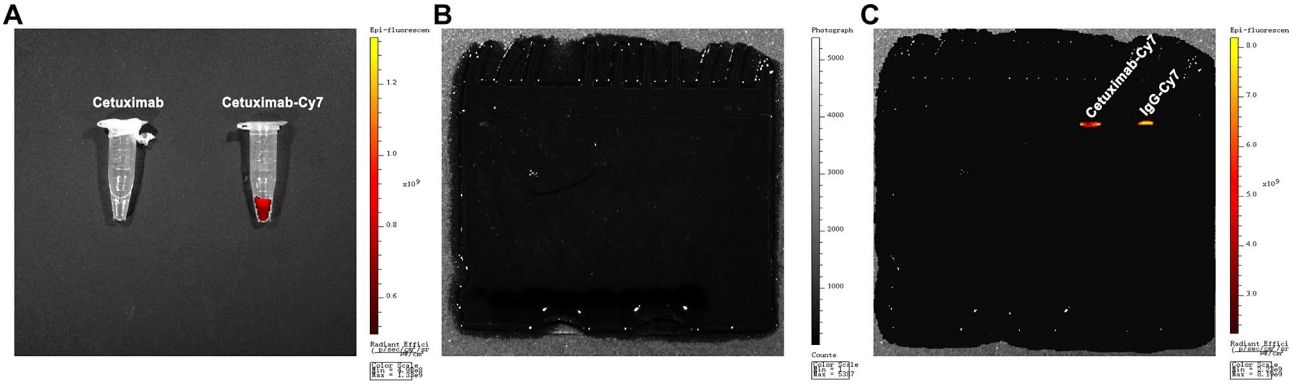


**Fig. 2** Characterization of cetuximab-Cy7 probe (**A**) The Cy7-labeled EGFR antibody solution was screened using NIRF imaging. SDS-PAGE of Cy7-labeled antibodies under (**B**) bright-field condition and (**C**) NIRF imaging. NIRF: near-infrared fluorescence; SDS-PAGE: sodium dodecyl sulfate - polyacrylamide gel electrophoresis; Cetuximab-Cy7: cetuximab-cyanine7; IgG-Cy7: immunoglobulin G-cyanine7

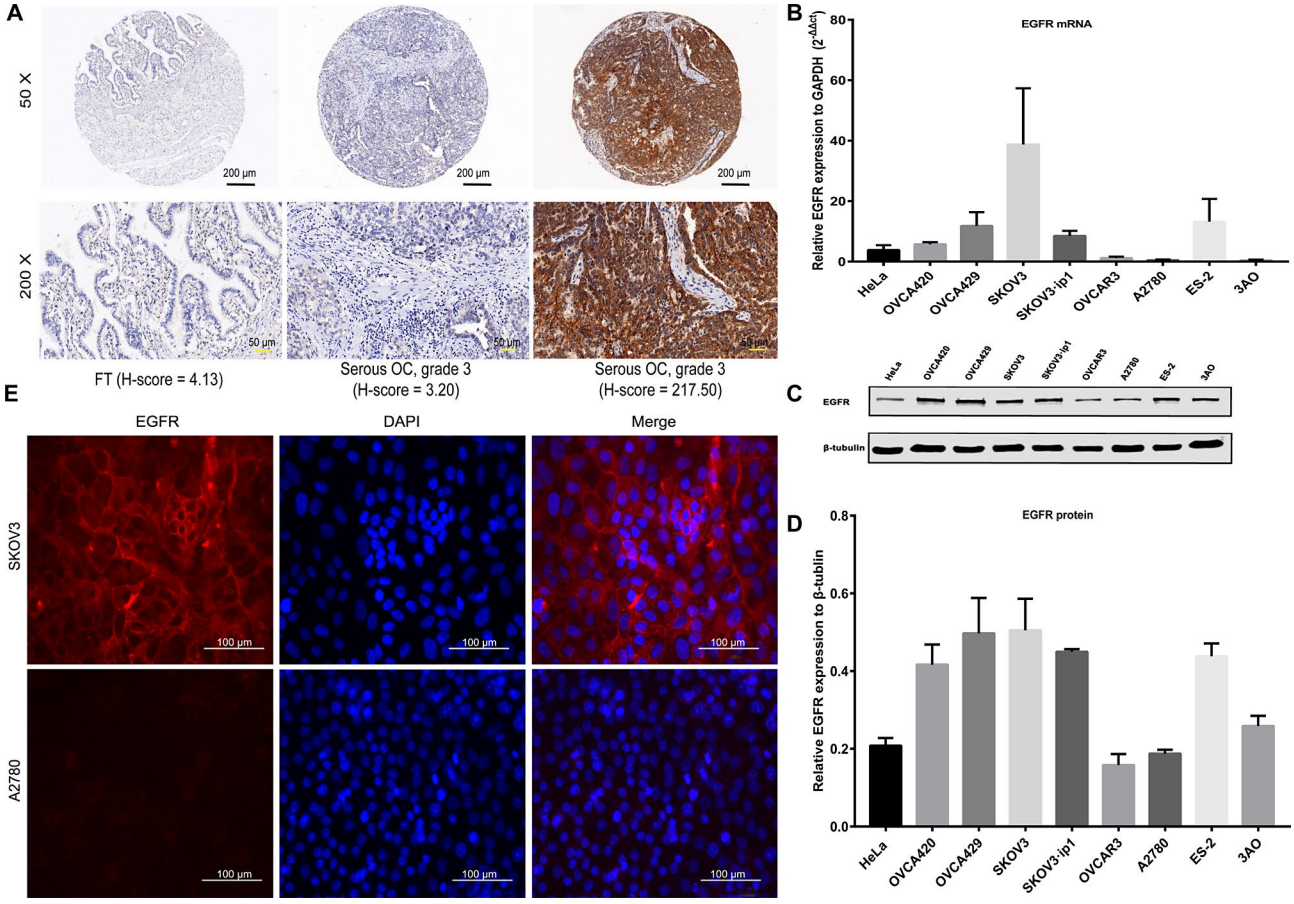


**Fig. 3** EGFR expression in OC tissues and cell lines. (**A**) IHC staining of EGFR protein in TMAs. FT tissue with a low H-score (4.13); a serous OC tumor (grade 3) with a low H-score (3.20); and a serous OC tumor (grade 3) with a high H-score (217.50). Black scale bar, 200 μm; yellow scale bar, 50 μm. (**B**) EGFR mRNA expression in OC cell lines was detected by qPCR. (**C**) WB of EGFR protein in OC cell lines and (**D**) quantification analyses. (**E**) IF staining of EGFR in OC SKOV3 cells (positive) and A2780 cells (negative). EGFR, red; DAPI, blue. Magnification 400×; white scale bar, 100 μm. OC: ovarian cancer; IHC: immunohistochemical; TMAs: tissue microarrays; FT: fallopian tube; qPCR: quantitative real-time PCR; WB: western blotting; IF: immunofluorescence; DAPI: 4′,6-diamidino-2-phenylindole

**Table 1** EGFR expression in FT and OC samples

| Group | Samples | EGFR expression [N (%)] | | χ2 | p value |
|---|---|---|---|---|---|
| | | Low (H-score ≤ 96.83) | High (H-score > 96.83) | | |
| FT tissues | 112 | 93 (83.0) | 19 (17.0) | 23.288 | 0.000 |
| OC tissues | 420 | 245 (58.3) | 175 (41.7) | | |

FT, fallopian tube; OC, ovarian cancer

The fluorescent signals in the 1.1 μg and 3.3 μg cetuximab-Cy7 groups were significantly weaker compared to the 10 μg and 30 μg groups (Fig. 4B). Starting from 96 hpi, the fluorescent signals in the 10 μg and 30 μg cetuximab-Cy7 groups were dominantly concentrated at the tumor site. Both the 10 μg and 30 μg cetuximab-Cy7 groups were able to specifically target the subcutaneous transplanted tumors, and the fluorescent signals in the 30 μg group were consistently stronger than those in other groups at each time point. Further, we compared the T/B ratio of cetuximab-Cy7 with that of PBS, free Cy7, and IgG-Cy7 with the same protein mass at the indicated time points (Fig. 5A-D). In the 1.1 μg cetuximab-Cy7 group, the T/B ratio was higher than that of the PBS group ($p=0.0113$), the free Cy7 group ($p=0.0011$), and the IgG-Cy7 group ($p=0.0456$) at 4 hpi. In the 3.3 μg cetuximab-Cy7 group, the T/B ratio was higher than that of the PBS group at 4 hpi ($p=0.0001$), 24 hpi ($p=0.0001$) and 48 hpi ($p=0.0013$), and the free Cy7 group ($p=0.0001$) at 4 hpi, 24 hpi ($p=0.0001$), 48 hpi ($p=0.0007$) and 144 hpi ($p=0.0006$), and IgG-Cy7 group at 4 hpi ($p=0.0001$), 24 hpi ($p=0.0001$) and 48 hpi ($p=0.0033$). In the 10 μg cetuximab-Cy7 group, the T/B ratio was significantly higher than that of the control groups at almost all monitoring points ($p\leq0.0010$). Except at 264 hpi, the T/B ratio of the 10 μg cetuximab-Cy7 group was higher than the PBS group and the free Cy7 group (both $p=0.0001$), while there was no statistical difference compared to the 10 μg IgG-Cy7 group ($p=0.1157$). In the 30 μg cetuximab-Cy7

**Table 2** EGFR expression features in OC patients (420 cases)

| Characteristics | *N* (%) | EGFR expression [*N* (%)] | | χ2 | *p* value |
|---|---|---|---|---|---|
| | | Low (H-score ≤ 96.83) | High (H-score > 96.83) | | |
| Age at diagnosis (years) | | | | 2.089 | 0.148 |
| ≤ 50 | 149 (35.5) | 80(53.7) | 69(46.3) | | |
| > 50 | 269 (64.0) | 164(61.0) | 105(39.0) | | |
| Unknown | 2 (0.5) | | | | |
| Menopause | | | | 0.954 | 0.329 |
| No | 150 (35.7) | 84(56.0) | 66(44.0) | | |
| Yes | 256 (61.0) | 156(60.9) | 100(39.1) | | |
| Unknown | 14 (3.3) | | | | |
| Histological subtypes | | | | 7.106 | 0.008* |
| Serous | 371 (88.3) | 209 (56.3) | 162 (43.7) | | |
| Nonserous | 44 (10.5) | 34 (77.3) | 10 ((22.7) | | |
| Unknown | 5 (1.2) | | | | |
| FIGO stage | | | | 2.706 | 0.439 |
| I | 43 (10.2) | 22 (51.2) | 21 (48.8) | | |
| II | 34 (8.1) | 23 (67.6) | 11 (32.4) | | |
| III | 291 (69.3) | 172 (59.1) | 119 (40.9) | | |
| IV | 18 (4.3) | 9 (50.0) | 9 (50.0) | | |
| Unknown | 34 (8.1) | | | | |
| Histological grade | | | | 13.344 | 0.001* |
| Grade 1 | 24 (5.8) | 6 (25.0) | 18 (75.0) | | |
| Grade 2 | 17 (4.0) | 13 (76.5) | 4 (23.5) | | |
| Grade 3 | 332 (79.0) | 197(59.3) | 135 (40.7) | | |
| Unknown | 47 (11.2) | | | | |
| Lymph node metastasis | | | | 0.106 | 0.744 |
| Negtive | 136 (32.4) | 81(59.6) | 55(40.4) | | |
| Positive | 76 (18.1) | 47(61.8) | 29(38.2) | | |
| Unknown | 208 (49.5) | | | | |
| Ascites (mL) | | | | 1.503 | 0.220 |
| < 500 | 87 (20.7) | 46 (52.9) | 41(47.1) | | |
| ≥ 500 | 213 (50.7) | 129 (60.6) | 84(39.4) | | |
| Unknown | 120 (28.6) | | | | |
| Preoperative CA125 (U/ml) | | | | | |
| < 35 | 28 (6.7) | 17(60.7) | 11(39.3) | 0.091 | 0.763 |
| ≥ 35 | 372 (88.5) | 215(57.8) | 157(42.2) | | |
| Unknown | 20 (4.8) | | | | |
| Residual tumor size (cm) | | | | | |
| ≤ 1 | 137 (32.6) | 67(48.9) | 70(51.1) | 14.266 | 0.000* |
| > 1 | 59 (14.1) | 46(78.0) | 13(22.0) | | |
| Unknown | 224 (53.3) | | | | |
| Platinum resistance | | | | | |
| No | 91 (21.7) | 44(48.4) | 47(51.6) | 0.782 | 0.377 |
| Yes | 35 (8.3) | 20(57.1) | 15(42.9) | | |
| Unknown | 294 (70.0) | | | | |
| Relapse | | | | | |
| No | 123 (29.3) | 50 (40.7) | 73 (59.3) | 15.991 | 0.000* |
| Yes | 141 (33.6) | 92 (65.2) | 49 (34.8) | | |
| Unknown | 156 (37.1) | | | | |
| Death | | | | 9.151 | 0.002* |
| No | 182 (43.3) | 94(51.6) | 88(48.4) | | |
| Yes | 142 (33.8) | 97(68.3) | 45(31.7) | | |
| Unknown | 96 (22.9) | | | | |

*$p < 0.05$. OC, ovarian cancer; FIGO, International Federation of Gynecology and Obstetrics; CA125, cancer antigen 125

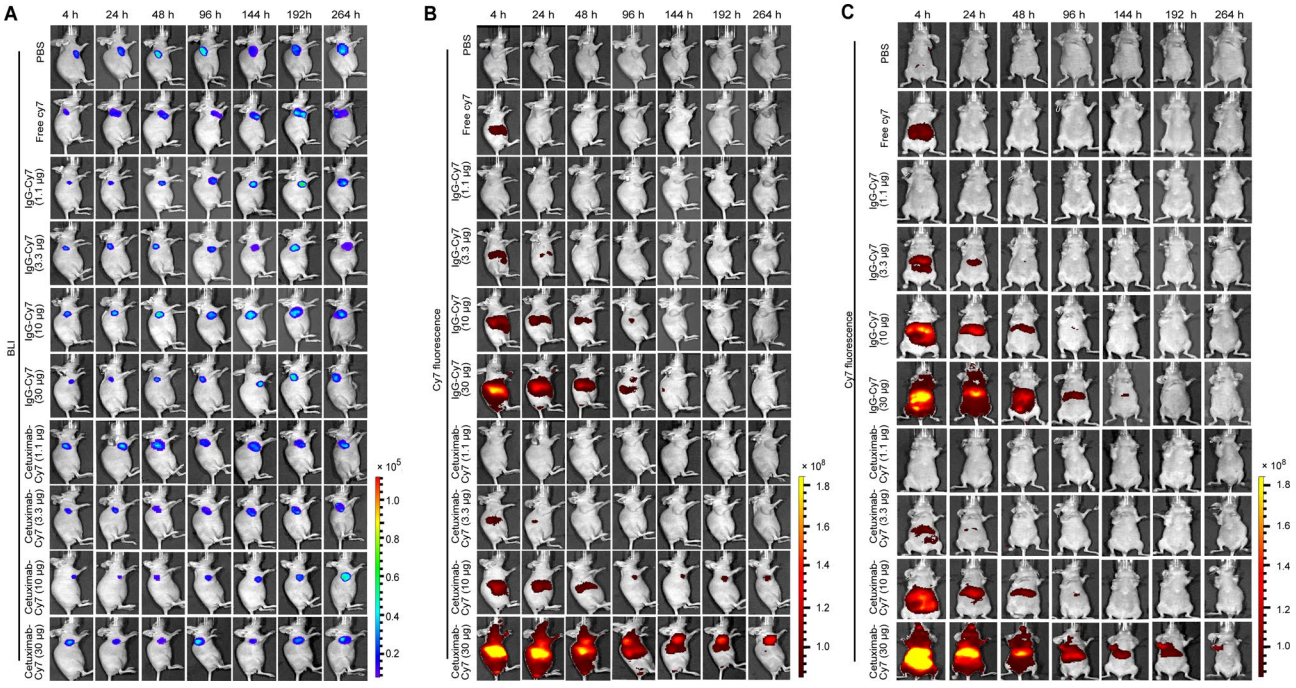


**Fig. 4** In vivo imaging of subcutaneous OC tumors and biodistribution of cetuximab-Cy7 probe. (**A**) BLI imaging was used to detect SKOV3-Luc OC tumor cells at 4, 24, 48, 96, 144, 192, and 264 h post-injection of cetuximab-Cy7. In vivo NIRF imaging of mice post-injection of cetuximab-Cy7 in (**B**) the lateral position and (**C**) the ventral position at the same timepoints. The control groups including PBS, free Cy7 dye and mouse isotype IgG-Cy7 were also used in our previous work [22]. The corresponding images in the control groups in Fig. 4A and B were reprinted with permission from reference 22. OC: ovarian cancer; BLI: bioluminescent; Cetuximab-Cy7: cetuximab-cyanine7; IgG-Cy7: immunoglobulin G-cyanine7; NIRF: near-infrared fluorescence; PBS: phosphate-buffered saline

group, the T/B ratio was significantly elevated compared to the control groups at each time point (all $p=0.0001$). Overall, the T/B ratio increased with the dose of the fluorescent imaging agent antibody. The T/B ratio of the 30 μg cetuximab-Cy7 group could distinguish that of the control groups at the indicated time points, suggesting that it may be a suitable imaging dose.

The cetuximab-Cy7 probe was first distributed throughout the body via the blood system and then gradually distributed to metabolic organs such as liver, spleen, and kidneys, with the strongest signals observed in the liver (Fig. 4C). As shown in Fig. 5F, the signal in the liver was highest at 4 hpi for the 30 μg cetuximab-Cy7 group and gradually decreased, approaching the tumor signal value at 96 hpi. Compared to the stable signal of the 30 μg IgG-Cy7 group (Fig. 5E), the signal value of 30 μg cetuximab-Cy7 in the tumor region continuously increased from 4 hpi, reaching a peak at 96 hpi, and then decreased. Combined with the lateral fluorescence imaging in Figs. 4B, we speculated that 24–96 hpi may be a suitable imaging time window for cetuximab-Cy7 probe.

### Ex vivo NIRF imaging and histological verification of EGFR binding

The EOC xenograft models in the study were sacrificed at 264 hpi. The organs of the mice and subcutaneous transplanted tumors were excised. Ex vivo NIRF imaging showed that fluorescent signals were strong in tumor and lung in the 30 μg cetuximab-Cy7 group, followed by liver (Fig. 6A). H&E staining of the tumor tissue indicated the formation of epithelial serous OC. IHC staining showed that EGFR was positively stained in the transplanted EOC tumor (Fig. 6B).

## Discussion

The advent of precision medicine is promising to effectively intervene the occurrence and progression of cancer. In recent decades, fluorescence imaging has been successfully applied to assist surgeons in detecting tumor margins and resecting micro-tumors during surgery [25]. Fluorescent dyes are mainly divided into three categories based on wavelength including traditional fluorescent dyes, NIR-I and NIR-II dyes. The NIR-I dyes are primarily organic small molecule fluorophores, such as cyanide dyes, fluorescein isothiocyanate, indocyanine green (ICG), and methylene blue. The dyes have wavelengths ranging from 650 to 900 nm, with high sensitivity, deep penetration, low absorption, low self-luminescence, and high spatial resolution. The NIR-II dyes have a longer wavelength, ranging from 1000 to 1700 nm, and deeper penetration [26].

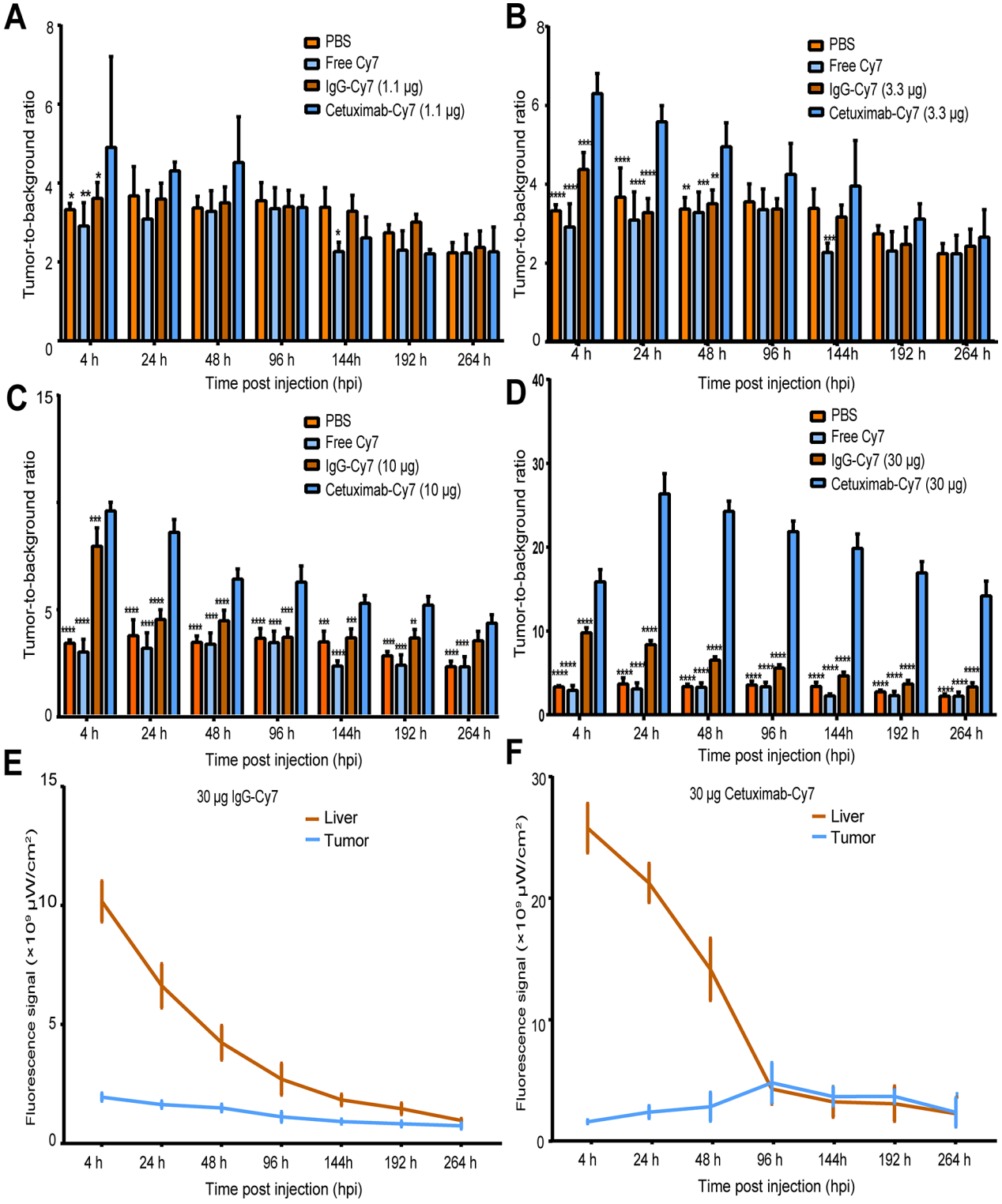


**Fig. 5** Quantification of the fluorescence intensity of in vivo NIRF imaging using cetuximab-Cy7 probe in OC tumor models. The T/B ratios for (**A**) 1.1 μg cetuximab-Cy7, (**B**) 3.3 μg cetuximab-Cy7, (**C**) 10 μg cetuximab-Cy7 and (**D**) 30 μg cetuximab-Cy7 groups at all time points. Quantification of fluorescence intensity of (**E**) 30 μg mouse isotype IgG-Cy7 and (**F**) 30 μg cetuximab-Cy7 groups were shown for tumor and liver ($n=3$). The mice were divided into 10 groups with 3 mice in each group, respectively intravenously injected with PBS, free Cy7, 1.1 μg, 3.3 μg, 10 μg, 30 μg dose of cetuximab-Cy7 or IgG-Cy7. *, $p<0.05$; **, $p<0.01$; ***, $p<0.001$; ****, $p<0.0001$. The control groups including PBS, free Cy7 dye and mouse isotype IgG-Cy7 were also used in our previous work [22]. The corresponding images in the control groups in Fig. 5A -E were reprinted with permission from reference 22. NIRF: near-infrared fluorescence; Cetuximab-Cy7: cetuximab-cyanine7; OC: ovarian cancer; T/B: tumor-to-background; IgG-Cy7: immunoglobulin G-cyanine7; PBS: phosphate-buffered saline; hpi: time post injection

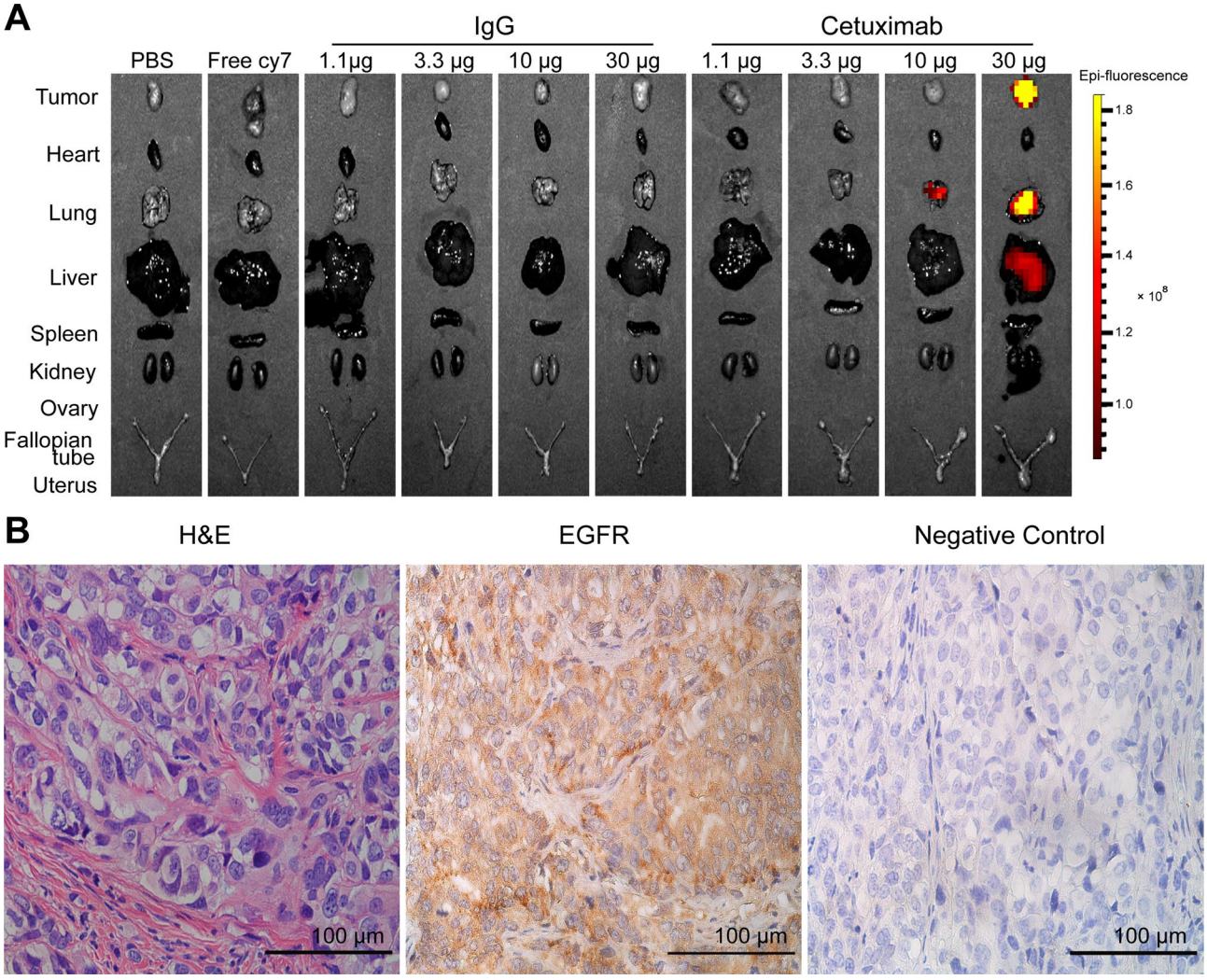


**Fig. 6** *Ex* vivo imaging and IHC staining of EGFR in OC tumors. (**A**) Ex vivo NIRF imaging of tumor and normal organs in different groups. (**B**) IHC staining of EGFR protein in OC tumor tissue. Magnification 400×; scale bar, 100 μm. The control groups including PBS, free Cy7 dye and mouse isotype IgG-Cy7 were also used in our previous work [22]. The corresponding images in the control groups in Fig. 6A were reprinted with permission from reference 22. IHC: immunohistochemical; OC: ovarian cancer; NIRF: near-infrared fluorescence; IgG: immunoglobulin G; PBS: phosphate-buffered saline; H&E, hematoxylin-eosin

NIRF imaging is preferred by researchers for in vivo real-time navigation due to the advantages of the dyes. For instance, ICG may help visualize the tumors to assist in pulmonary metastasectomy for hepatocellular carcinoma [27]. However, when ICG was employed to detect OC metastases during surgery, no difference in the T/B ratio was observed between malignant tissues and benign lesions, with a false-positive rate of up to 62% [28]. It seems that the passive targeting imaging of ICG based on the enhanced permeability and retention effect may be not suitable for detecting OC metastases, and specific imaging agents utilizing OC-targeting ligands are needed.

The main strategy of active targeting imaging is based on the binding of targeted ligands of fluorescent molecular probes to receptors on tumor cells. Therefore, selecting specific and high-affinity targets is the key to constructing such imaging agents. An increasing number of studies are applying fluorescent probes targeting biomarkers of EOC, such as cancer antigen 125 (CA125) [29], cluster of differentiation 24 (CD24) [30] and FR-a [10, 11] in the preclinical stage and clinical trials [5]. For instance, Kleinmanns et al. demonstrated that CD24-targeted FGS improved tumor resection in xenograft models of EOC [30].

EGFR is a broad-spectrum tumor marker. Fluorescence imaging targeting EGFR for the detection of head and neck squamous cell carcinoma (HNSCC) has been reported [31–33]. Specific commercialized antibodies targeting EGFR can achieve sub-millimeter resolution for the identification of HNSCC [31]. Fluorescently labeled anti-human EGFR recombinant antibody single chain

antibody fragment (scFv) could be used to rapid determine of tumor boundaries in freshly isolated tissue and find metastases in lymph nodes in lung cancer [34]. In the study, we investigated EGFR targeting EOC in vitro and in vivo due to its wide expression in kinds of tumors and commercially available EGFR antibodies.

Herein, EGFR is highly expressed in EOC tissues, especially in serous subtype, serving as a specific target for EOC. Cetuximab is a chimeric IgG1 monoclonal antibody targeting EGFR and consisting of murine-derived variable regions of the light and heavy chains (responsible for recognizing and binding to EGFR) and human-derived constant regions, designed to reduce the immune response against the murine components in the human body. A NIR fluorescent molecular probe was constructed using cetuximab as the carrier, and identified its successful construction by NIRF imaging and SDS-PAGE. We established a serous OC subcutaneous xenograft model using SKOV3-Luc cell line expressing EGFR and BALB/c female nude mice, and explored the distribution and targeting efficacy of cetuximab-Cy7 in vivo. BALB/c nude mice lack mature T lymphocytes resulting in low cellular immune function, and possess normal B lymphocytes, but had poor humoral immune function mainly producing IgM antibody and a small amount of IgG antibody, which were also employed in other studies to investigate fluorescence imaging using cetuximab-associated antibody [35–37]. In the study, NIRF imaging results showed that cetuximab-Cy7 probe can specifically target OC tumors and 30 μg cetuximab-Cy7 may be a suitable imaging dose. During the experiments, no acute or chronic toxic symptoms were observed in the mice. Although there may be some cross-reaction in mouse tissues with cetuximab when BALB/c nude mice received injection with cetuximab, it may not have apparent effect on the experiment results. In the future, peritoneal or in situ tumor models which better simulate the real situation in humans deserve to be explored in related research. Collectively, these findings suggest that the NIR fluorescent molecular probe cetuximab-Cy7 can specifically target serous OC xenografts with good tolerance.

This study has some limitations, but also some prospects. The IHC results showed that less than half of the EOC patients possessed higher expression of EGFR, but no targets are ideally expressed in all patients with EOC, and therefore the investigation of new specific targets still remains an important issue. Given the relatively limited sample size in the study, our clinicopathological analyses showed that EGFR expression had no statistically significant correlation with platinum resistance, which may deserve expanding the sample size in the future. It could be speculated that EGFR may be associated with cisplatin resistance according to many reports [16–21]. EGFR antibodies would be used in magnetic hyperthermia for integrated diagnosis and treatment of OC patients with cisplatin resistance [38], and the penetration ability of probes would be increased to reach the deep tumor sites through modification [39]. Additionally, as full-length antibody with large molecule, cetuximab has a long retention time in organs and is difficult to penetrate lymph nodes. We may conjugate small molecule antibodies, such as fragment of antigen binding and scFv, with NIR dyes to construct probes to shorten imaging time, decrease non-specific imaging and explore imaging of lymph nodes. In summary, cetuximab, as a commercially approved antibody already in clinical use, holds promise for application in NIRF imaging of EOC and possesses translational value for clinical practice.

## Supplementary Information

The online version contains supplementary material available at https://doi.org/10.1186/s13048-024-01547-5.

Supplementary Material 1

Supplementary Material 2

### Acknowledgements

The authors would like to thank Tao Liu and Xinyu Ling from State Key Laboratory of Natural and Biomimetic Drugs, School of Pharmaceutical Sciences, Peking University for the assistance in antibody labeling with cetuximab and the in vivo fluorescence imaging, and Beihua Kong and Cunzhong Yuan from Department of Obstetrics and Gynecology, Qilu Hospital of Shandong University for providing the tissue microarrays used in the study.

### Author contributions

C.Z. designed the study, performed data analysis and wrote the manuscript. H.Y.C. and X.Y. performed data analysis. S.D. and Y.F.W. collected the clinical data. H.C., X.H.C. and Y.L. supervised the experiments and reviewed the manuscript.

### Funding

This work was supported by the National Key Research and Development Program of China (No. 2022YFC2704204), the Beijing Natural Science Foundation (No. 7222204; No. 7222202) and National Key Research and Development Program of China (No.2016YFA0201400).

### Data availability

No datasets were generated or analysed during the current study.

## Declarations

### Ethics approval and consent to participate

This experiment was approved by the Medical Ethics Committee of Peking University People's Hospital (No.2016PHC078), and all patients signed informed consent.

### Consent for publication

Not required.

### Competing interests

The authors declare no competing interests.

### Author details

[1]Department of Obstetrics and Gynecology, Peking University People's Hospital, No. 11 Xizhimen South Str., Xicheng District, Beijing 100044, China

Received: 22 July 2024 / Accepted: 27 October 2024

Published online: 14 November 2024

**References**


1. Siegel RL, Giaquinto AN, Jemal A. Cancer statistics, 2024. CA Cancer J Clin. 2024;74:12–49.
2. du Bois A, Reuss A, Pujade-Lauraine E, Harter P, Ray-Coquard I, Pfisterer J. Role of surgical outcome as prognostic factor in advanced epithelial ovarian cancer: a combined exploratory analysis of 3 prospectively randomized phase 3 multicenter trials: by the Arbeitsgemeinschaft Gynaekologische Onkologie Studiengruppe Ovarialkarzinom (AGO-OVAR) and the Groupe d'Investigateurs Nationaux Pour Les Etudes des Cancers de l'Ovaire (GINECO). Cancer. 2009;115:1234–44.
3. Eisenkop SM, Friedman RL, Wang HJ. Complete cytoreductive surgery is feasible and maximizes survival in patients with advanced epithelial ovarian cancer: a prospective study. Gynecol Oncol. 1998;69:103–8.
4. Lauwerends LJ, van Driel P, Baatenburg de Jong RJ, Hardillo JAU, Koljenovic S, Puppels G, et al. Real-time fluorescence imaging in intraoperative decision making for cancer surgery. Lancet Oncol. 2021;22:e186–95.
5. Sun C, Huang Y, Jiang C, Li Z. Updates on fluorescent probes and open-field imaging methods for fluorescence-guided cytoreductive surgery for epithelial ovarian cancer: a review. BJOG. 2022;129(Suppl 2):50–9.
6. Kalli KR, Oberg AL, Keeney GL, Christianson TJ, Low PS, Knutson KL, et al. Folate receptor alpha as a tumor target in epithelial ovarian cancer. Gynecol Oncol. 2008;108:619–26.
7. Markert S, Lassmann S, Gabriel B, Klar M, Werner M, Gitsch G, et al. Alpha-folate receptor expression in epithelial ovarian carcinoma and non-neoplastic ovarian tissue. Anticancer Res. 2008;28:3567–72.
8. Siu MK, Kong DS, Chan HY, Wong ES, Ip PP, Jiang L, et al. Paradoxical impact of two folate receptors, FRalpha and RFC, in ovarian cancer: effect on cell proliferation, invasion and clinical outcome. PLoS ONE. 2012;7:e47201.
9. Toffoli G, Cernigoi C, Russo A, Gallo A, Bagnoli M, Boiocchi M. Overexpression of folate binding protein in ovarian cancers. Int J Cancer. 1997;74:193–8.
10. Randall LM, Wenham RM, Low PS, Dowdy SC, Tanyi JL. A phase II, multicenter, open-label trial of OTL38 injection for the intra-operative imaging of folate receptor-alpha positive ovarian cancer. Gynecol Oncol. 2019;155:63–8.
11. Tanyi JL, Randall LM, Chambers SK, Butler KA, Winer IS, Langstraat CL, et al. A phase III study of pafolacianine injection (OTL38) for intraoperative imaging of Folate receptor-positive ovarian Cancer (study 006). J Clin Oncol. 2023;41:276–84.
12. Wilken JA, Badri T, Cross S, Raji R, Santin AD, Schwartz P, et al. EGFR/HER-targeted therapeutics in ovarian cancer. Future Med Chem. 2012;4:447–69.
13. Alper O, Bergmann-Leitner ES, Bennett TA, Hacker NF, Stromberg K, Stetler-Stevenson WG. Epidermal growth factor receptor signaling and the invasive phenotype of ovarian carcinoma cells. J Natl Cancer Inst. 2001;93:1375–84.
14. Lafky JM, Wilken JA, Baron AT, Maihle NJ. Clinical implications of the ErbB/epidermal growth factor (EGF) receptor family and its ligands in ovarian cancer. Biochim Biophys Acta. 2008;1785:232–65.
15. Forlani L, De Cecco L, Simeon V, Paolini B, Bagnoli M, Cecere SC, et al. Biological and clinical impact of membrane EGFR expression in a subgroup of OC patients from the phase IV ovarian cancer MITO-16A/MANGO-OV2A trial. J Exp Clin Cancer Res. 2023;42:83.
16. Poursheikhani A, Yousefi H, Tavakoli-Bazzaz J, Seyed HG. EGFR Blockade reverses Cisplatin Resistance in Human epithelial ovarian Cancer cells. Iran Biomed J. 2020;24:370–8.
17. Zhao J, Tan W, Zhang L, Liu J, Shangguan M, Chen J, et al. FGFR3 phosphorylates EGFR to promote cisplatin-resistance in ovarian cancer. Biochem Pharmacol. 2021;190:114536.
18. Zhang Y, Tao L, Fan LX, Huang K, Luo HM, Ge H, et al. Cx32 mediates cisplatin resistance in human ovarian cancer cells by affecting drug efflux transporter expression and activating the EGFR–Akt pathway. Mol Med Rep. 2019;19:2287–96.
19. Zhang M, Cong Q, Zhang XY, Zhang MX, Lu YY, Xu CJ. Pyruvate dehydrogenase kinase 1 contributes to cisplatin resistance of ovarian cancer through EGFR activation. J Cell Physiol. 2019;234:6361–70.
20. Li D, Wu QJ, Bi FF, Chen SL, Zhou YM, Zhao Y, et al. Effect of the BRCA1-SIRT1-EGFR axis on cisplatin sensitivity in ovarian cancer. Am J Transl Res. 2016;8:1601–8.
21. Yue P, Zhang X, Paladino D, Sengupta B, Ahmad S, Holloway RW, et al. Hyperactive EGF receptor, Jaks and Stat3 signaling promote enhanced colony-forming ability, motility and migration of cisplatin-resistant ovarian cancer cells. Oncogene. 2012;31:2309–22.
22. Zhang C, Ling X, Guo Y, Yuan C, Cheng H, Ye X, et al. Evaluation of COC183B2 antibody targeting ovarian cancer by near-infrared fluorescence imaging. Chin J Cancer Res. 2019;31:673–85.
23. Azim HA Jr., Peccatori FA, Brohee S, Branstetter D, Loi S, Viale G, et al. RANK-ligand (RANKL) expression in young breast cancer patients and during pregnancy. Breast Cancer Res. 2015;17:24.
24. El-Sayed A, Bernhard W, Barreto K, Gonzalez C, Hill W, Pastushok L, et al. Evaluation of antibody fragment properties for near-infrared fluorescence imaging of HER3-positive cancer xenografts. Theranostics. 2018;8:4856–69.
25. Chi C, Du Y, Ye J, Kou D, Qiu J, Wang J, et al. Intraoperative imaging-guided cancer surgery: from current fluorescence molecular imaging methods to future multi-modality imaging technology. Theranostics. 2014;4:1072–84.
26. Kashiwagi S, Choi HS. Ovarian cancer-targeted near-infrared fluorophores for fluorescence-guided surgery. Ann Transl Med. 2023;11:274.
27. Wang Z, Yang F, Zhao X, Mi J, Sun L, Kang N et al. Outcome of near-infrared fluorescence-navigated pulmonary metastasectomy for hepatocellular carcinoma. Eur J Cardiothorac Surg. 2022;62(5):ezac270.
28. Tummers QR, Hoogstins CE, Peters AA, de Kroon CD, Trimbos JB, van de Velde CJ, et al. The value of Intraoperative Near-Infrared fluorescence imaging based on enhanced permeability and Retention of Indocyanine Green: feasibility and false-positives in Ovarian Cancer. PLoS ONE. 2015;10:e0129766.
29. Fung K, Sharma SK, Keinanen O, Roche KL, Lewis JS, Zeglis BM. A molecularly targeted intraoperative Near-Infrared fluorescence imaging Agent for High-Grade Serous Ovarian Cancer. Mol Pharm. 2020;17:3140–7.
30. Kleinmanns K, Fosse V, Bjorge L, McCormack E. The emerging role of CD24 in Cancer Theranostics-A Novel Target for fluorescence image-guided surgery in Ovarian Cancer and Beyond. J Pers Med. 2020;10.
31. Rosenthal EL, Warram JM, de Boer E, Chung TK, Korb ML, Brandwein-Gensler M, et al. Safety and Tumor specificity of Cetuximab-IRDye800 for Surgical Navigation in Head and Neck Cancer. Clin Cancer Res. 2015;21:3658–66.
32. Heath CH, Deep NL, Sweeny L, Zinn KR, Rosenthal EL. Use of panitumumab-IRDye800 to image microscopic head and neck cancer in an orthotopic surgical model. Ann Surg Oncol. 2012;19:3879–87.
33. Gao RW, Teraphongphom N, de Boer E, van den Berg NS, Divi V, Kaplan MJ, et al. Safety of panitumumab-IRDye800CW and cetuximab-IRDye800CW for fluorescence-guided surgical navigation in head and neck cancers. Theranostics. 2018;8:2488–95.
34. Li C, Mi J, Wang Y, Zhang Z, Guo X, Zhou J, et al. New and effective EGFR-targeted fluorescence imaging technology for intraoperative rapid determination of lung cancer in freshly isolated tissue. Eur J Nucl Med Mol Imaging. 2023;50:494–507.
35. Amini A, Safdari Y, Tash Shamsabadi F. Near-Infrared fluorescence imaging of EGFR-Overexpressing tumors in the mouse xenograft model using scFv-IRDye800CW and Cetuximab-IRDye800CW. Mol Imaging. 2022;2022:9589820.
36. Wang L, Liang M, Xiao Y, Chen J, Mei C, Lin Y, et al. NIR-II Navigation with an EGFR-Targeted probe improves Imaging Resolution and Sensitivity of detecting micrometastases in esophageal squamous cell carcinoma xenograft models. Mol Pharm. 2022;19:3563–75.
37. Zhu CN, Chen G, Tian ZQ, Wang W, Zhong WQ, Li Z et al. Near-Infrared fluorescent ag(2) Se-Cetuximab Nanoprobes for targeted imaging and therapy of Cancer. Small. 2017;13.
38. Sadhukha T, Wiedmann TS, Panyam J. Inhalable magnetic nanoparticles for targeted hyperthermia in lung cancer therapy. Biomaterials. 2013;34:5163–71.
39. Antaris AL, Chen H, Cheng K, Sun Y, Hong G, Qu C, et al. A small-molecule dye for NIR-II imaging. Nat Mater. 2016;15:235–42.


## Publisher's note